Pergamon

Int. J. Solids Structures Vol. 33, No. 29, pp. 4379–4393, 1996

0020–7683/96 $15.00 + .00

0020–7683(95)00236–7

A DAMAGE MECHANICS MODEL FOR COMPRESSION STRENGTH OF COMPOSITES

EVER J. BARBERO
Mechanical and Aerospace Engineering, West Virginia University, Morgantown, WV 26506-6106, U.S.A.

and

JOHN TOMBLIN
Aerospace Engineering, Witchita State University, Witchita, KS, U.S.A.

(*Received* 16 *March* 1995; *in revised form* 4 *October* 1995)

Abstract—A compression strength model based on damage mechanics and a Gaussian distribution of fiber misalignment is presented. The model uses only three material parameters that can be measured by well established methodologies. The compression strength and all the parameters that enter in the model were measured for the same materials. Predicted values are compared to experimental data for eleven different E-glass reinforced pultruded composites. Theoretical arguments are provided to support the use of damage mechanics and very good correlation is found between theory and experiments. Copyright © 1996 Elsevier Science Ltd.

INTRODUCTION

Many models have been proposed trying to improve the prediction of compression strength of composites by Rosen (1965). The literature is divided into two schools of thought: fiber micro-buckling models (Rosen, 1965; Wang, 1978), and kink band formation models (Budiansky, 1983; Budiansky and Fleck, 1993; Lagoudas and Saleh, 1993), etc. Two comprehensive reviews (Shuart, 1985; Camponeschi, 1990) cover much of the literature. To the best of our knowledge, none of the existing models can be correlated with experimental data without introducing a semi-empirical parameter or empirical judgment about the value of fiber misalignment to be used (Yurgartis, 1992; Haberle and Matthews, 1994). Usually, the fiber misalignment is taken as the semi-empirical parameter and it is set to a reasonable value so that the model predictions match the experimental data (Wang, 1978; Piggott, 1981; Hahn and Williams, 1986; Mrse and Piggott, 1990), etc. By performing tests at different temperatures, effectively changing the shear response, Wang showed that after the fiber misalignment is found empirically (by fitting measured strength data) it can be considered constant for a material.

However, it is well known that there is not a unique value for fiber misalignment for all the fibers (Yurgartis, 1987) but rather a Gaussian distribution of misalignment (Tomblin, 1994). The standard deviation of the normal distribution has been used (Haberle and Matthews, 1994; Kiriakides *et al.*, 1995), as a single misalignment value in the theoretical models. The standard deviation of the half normal distribution has been used also (Haberle and Matthews, 1994) for the same purpose. From a probabilistic point of view, the standard deviation is a measure of the dispersion of the distribution but it is not a measure representative of the misalignment of all the fibers (population). Instead, the expected value of a distribution is a representative measure of the population.

In this paper, continuous damage mechanics (Kachanov, 1990) is used to combine the Gaussian distribution of misalignment with a simple model for compression strength. Data and theoretical arguments are shown to support the assumption of progressive failure via fiber microbuckling. The resulting model has no semi-empirical parameters. All the physical parameters included in the model were measured for eleven different materials. The correlation with compression strength data is very good.

In fiber micro-buckling models, it is assumed that buckling of the fibers initiates a process that leads to the collapse of the material (Rosen, 1965). Rosen's model has been refined with the addition of initial fiber misalignment and non-linear shear stiffness (Wang, 1978; Hahn and Williams, 1986; Yeh and Teply, 1988; Wisnom, 1990), etc. The detrimental influence of fiber misalignment has been experimentally demonstrated (Yurgartis, 1992; Mrse and Piggott, 1990). The assumption of recent models is that fiber micro-buckling of perfectly aligned fibers (Rosen's model) is an imperfection sensitive problem. Therefore, small amounts of imperfection (misalignment) could cause large reductions in the buckling load, and thus the reduction of the compression strength with respect to Rosen's prediction. Using a linear shear response for the composite, Maewal (1981) concluded that fiber micro-buckling is not imperfection sensitive. The authors have shown (Tomblin, 1994) that imperfection sensitivity occurs only for composites with non-linear shear response. The effect of initial shear stiffness on the compression strength has been studied experimentally (Yurgartis, 1992; Crasto and Kim, 1990, 1992a,b), concluding that higher initial shear stiffness correlates with higher compression strength.

A new approach to micro-buckling in which the composite is treated as an inhomogeneous two-dimensional continuum with spatial variation of material properties (Lagoudas *et al.*, 1991), results in a knock down factor that improves Rosen's formula to results generally closer to experimental observations. Rosen's, as well as most other models in the literature, treat the composite as a two-dimensional arrangement of square fibers separated by a matrix. The fiber-matrix flat arrangement is implicitly assumed to be in a state of plane stress because the constitutive equations used are the one-dimensional Hooke's law for extension as well as shear. The non-uniform spacing among fibers has been incorporated following a more realistic approach (Chung and Weitsman, 1994, 1995). While the literature on compression strength is extensive, there is no model in the literature that has been validated by measuring all the parameters involved from the same specimen. Usually, the shear response is obtained from $\pm 45^{\circ}$ samples and the compression strength from unidirectional samples, which may have slightly different misalignment, volume fraction, etc. Furthermore, samples are not subjected to a pure state of shear but to non-uniform shear. Therefore, one of the objectives of the work presented here is to develop and validate a model using material data from the same sample that is tested in compression. We found that the damage mechanics formulation yields an elegant and accurate model for compression strength that incorporates the statistical data of fiber misalignment in a well defined fashion.

MATERIALS AND SAMPLE PREPARATION

Cylindrical rods (9.2 mm nominal diameter) were pultruded by Creative Pultrusions, Inc. using three different resins, three different fiber types, and three fiber volume fractions. Each resin, fiber, and volume fraction was labeled, so that each resulting material is uniquely identified with a three-letter code. The first letter indicates the fiber volume fraction, the second letter the resin type, and the third letter the fiber type. The resins used were (A) Ashland 2036C Polyester, (B) D-1419 Vinyl Ester, and (C) 2036C with added styrene to increase the shrinkage and brittleness. The fibers were (A) 13 micron diameter OC 102-AA-56 yield [yard/lb], (B) 23 micron OC 366-AD-113 yield, and (C) 17 micron OC 366-AC-250 yield E-glass, all supplied by Owens Corning. Three values of fiber volume fraction were obtained for each fiber-matrix combination simply by starting the pultrusion with the highest volume fraction and subsequently cutting some roving ends to lower the volume fraction. The highest volume fraction (labeled A) corresponds to the maximum that could be pultruded. The fiber volume fraction cannot be kept constant when changing fiber type (each having a different yield) because an integer number of roving ends must be used in pultrusion. The number roving, yield, and resulting fiber volume fractions are shown in Table 1.

A rod geometry was chosen because it is the simplest shape that can be pultruded. To limit the amount of testing, and the number of variables active in the investigation, only

Table 1. Characteristics of the fiber reinforcement for all materials produced

Material Reference code	Volume fraction (%)	Number of roving	Yield [yard/lb]	Fiber diameter [microns]
CAA	40.2	8	56	13
CAB	43.0	17	113	23
CAC	43.9	39	256	27
CBA	40.2	8	56	13
CBB	43.0	17	113	23
CBC	43.9	39	256	27
CCA	40.2	8	56	13
CCB	43.0	17	113	23
CCC	43.9	39	256	27
ACA	55.2	11	56	13
BCA	50.2	10	56	13
CBB*	43.0	—	113	23

* Rectangular sample.

eleven material combinations were used of the twenty-seven produced. The eleven materials were chosen as follows. Keeping the volume fraction constant and using three fibers and three resins yields nine materials. Then, holding the fiber and resin unchanged while varying the volume fraction gives two additional materials for a total of eleven. The void content for each material was checked optically using a video analysis system and found to be less than 2% in all cases. Previous experimental evidence (Tang, 1987) indicates that the compression strength is not affected by void contents below 3%. The fiber coating was compatible with the resins used. Contradictions arise with respect to the role in which fiber-matrix adhesion affects compression strength. Using different fiber surface treatments, Madhukar and Drzal (1992) show that the compression strength is very sensitive to fiber-matrix adhesion. This result appears to be directly in contradiction to the experimental findings of Hahn and Williams (1986) in which the bond strength was characterized by acoustic emissions and by Yurgartis (1992) who used different fiber surface treatments. Although the role of fiber-matrix adhesion with respect to compression strength needs additional investigation, it appears that, as long as the fiber surface treatment is compatible with the matrix, fiber-matrix adhesion should not affect the compression strength. Hence, for this work, fiber-matrix failure was assumed negligible since the fiber-matrix systems were compatible and the appropriate surface treatment for the fibers was used.

Although this study concentrates on pultruded E-glass composites, the materials used covered a wide range of materials commonly used by the pultrusion industry. The 113 yield and 250 yield were direct-draw roving ends with low micro-catenary while the 56 yield was a multi-end roving with higher micro-catenary. The polyester and vinyl ester resins have different shrinkage and shear stiffness. The third resin, polyester with double amount of added styrene, showed increased shrinkage and brittleness. The fiber volume fractions used represent typical values of commercially pultruded composites. Material production was performed with standard equipment at a commercial plant.

SHEAR STIFFNESS MEASUREMENTS

The torsion test was chosen for determination of shear behavior because of the circular geometry of the specimens. The torsion test has been used successfully for pultruded composites in the past (Sonti and Barbero, 1995). The rod samples were twisted at a rate of 4–8 deg. per minute, which was found to be fast enough to prevent any viscoelastic effects, yet slow enough to prevent high modulus readings resulting from a high rate of loading. The shear stress-strain response was found to be non-linear elastic as shown in Fig. 1. The following equation is proposed to represent the stress-strain response

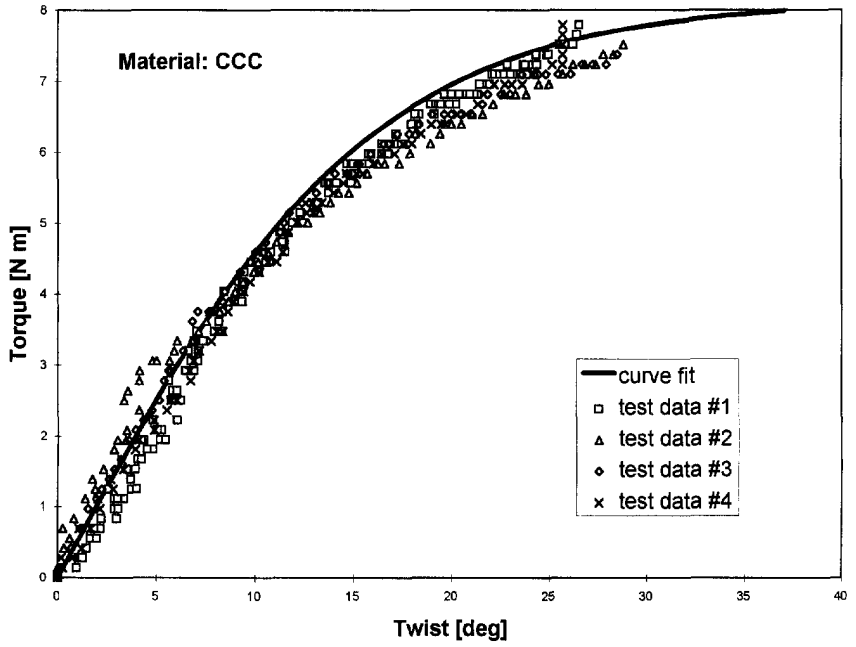

Fig. 1. Hyperbolic tangent fit of the experimental shear stress-strain response. Four independent tests shown.

$$\tau = \tau_u \tanh\left(\frac{G_{LT}}{\tau_u}\gamma\right) \tag{1}$$

where G_{LT} is the initial shear stiffness and τ_u is the asymptotic value of the shear stress in Fig. 1. Both G_{LT} and τ_u are computed from the measured torque vs angle of twist experimental data, modeling the stress strain curve with eqn (1). The initial shear stiffness G_{LT} is obtained from a linear regression of the linear portion of the curve. Then, eqn (1) is integrated over the cross section of the sample to obtain the predicted torque vs angle of twist function. The asymptotic value of the shear stress τ_u is obtained by comparing the predicted and experimental asymptotic values of torque.

Although the polynomial expansions (Sun and Jun, 1993) fit the experimental data, they do not represent the material correctly for negative shear strains (see Fig. 2), as they should since the shear stiffness is independent of the sign. Then, in the stability analysis,

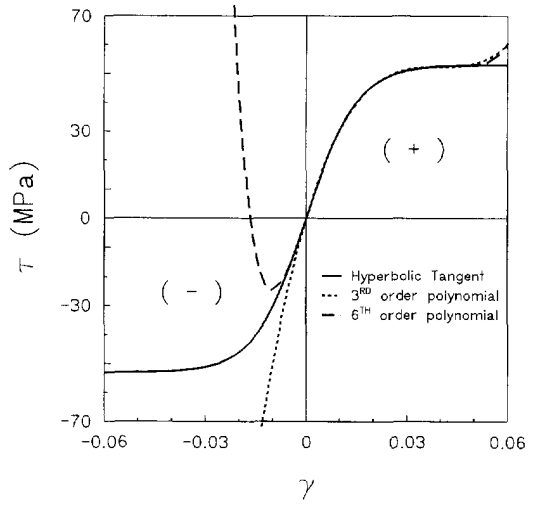

Fig. 2. Polynomial equations representing the shear stress-strain response.

Table 2. Experimental and predicted shear response

Material reference code	G_{LT}[GPa] Experimental	G_{LT}[GPa] Inverse rule of mixtures	G_{LT}[GPa] Periodic microstruct. formula	τ_u[GPa] Experimental
CAA	3.462(±0.536)	2.645	3.384	40.57(±2.66)
CAB	3.043(±0.182)	2.775	3.589	37.86(±4.49)
CAC	3.383(±0.112)	2.820	3.658	38.53(±2.08)
CBA	4.223(±0.213)	2.771	3.487	43.09(±3.07)
CBB	4.224(±0.119)	2.907	3.697	43.09(±1.30)
CBC	4.268(±0.251)	2.954	3.768	42.75(±0.49)
CCA	3.487(±0.359)	2.470	3.178	43.33(±5.08)
CCB	3.628(±0.329)	2.591	3.372	42.06(±2.10)
CCC	3.487(±0.354)	2.633	3.438	39.86(±2.27)
ACA	4.914(±0.432)	3.304	4.467	43.63(±2.62)
BCA	4.703(±0.133)	2.966	3.957	42.10(±2.00)
CBB	4.223(±0.386)*	2.907	3.697	54.77(±5.57)*

*Iosipescu shear test.

a polynomial expansion produces an asymmetric bifurcation point, which is physically unrealistic. Although a polynomial expansion in terms of the absolute value of the shear strain could be used, this would make the problem analytically intractable.

The experimental values of G_{LT} and τ_u are shown in Table 2. For the micromechanical predictions, the fiber shear modulus used was $G_f = 29.47$ GPa. The resin shear modulus was measured from 9.2 mm resin rods produced with resin taken out of the pultrusion resin-bath during production of the composite rods. Resin was poured into 9.2 mm quartz tubes and cured in an oven at approximately the same temperature recorded by thermocouples in the pultrusion die.

As expected, the predictions of G_{LT} by the inverse rule of mixtures are well below the experimental values. The periodic micro-structure formula (Luciano and Barbero, 1994), still a lower bound, provides a better approximation of the initial shear stiffness. However, the model predictions developed in Section 8 use the experimental values. The discrepancy between the experimental data and the periodic micro-structure formula can be partially explained taking into account that neat resin properties are different of *in-situ* resin properties. This is because of the different polymer morphology obtained while curing the resin in the presence of the surface of the fibers and the effect of the fiber coating on the polymerization reaction.

MISALIGNMENT MEASUREMENTS

An optical technique proposed by Yurgartis (1987) was used to measure the misalignment angle of each fiber in the cross section. The technique consists of cutting the composite at an angle and measuring the major axis of the ellipse formed by the intersection of a cylindrical fiber with the cutting plane. The misalignment angle is computed from the major axis length, the fiber diameter (which can be measured as the minor axis of the ellipse), and the angle of the cutting plane.

Yurgartis determined the cutting angle by assuming that the distribution of fiber misalignment was symmetric. In this investigation, we were able to accurately measure the angle of cut by measuring the major and minor axes of the ellipse formed by the rod specimen (the angle of cut varied from sample to sample around 10°). As a consequence, it was possible to prove Yurgartis' assumption of normality of the fiber distribution by using two statistical tests, the cumulative function distribution (Fig. 3) and the transformed frequency data on a probability plot (Fig. 4). The normal distribution of misalignment is given by

$$f(x) = \frac{1}{\Sigma\sqrt{2\pi}} \exp\left(\frac{-x^2}{2\Sigma^2}\right); \quad -\infty < x < \infty \tag{2}$$

where Σ is the standard deviation and x is the continuous random variable, in this case

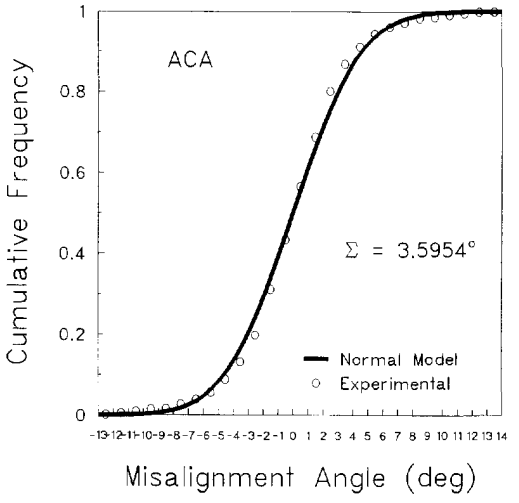

Fig. 3. Cumulative frequency plot of the experimental misalignment data and the normal distribution model.

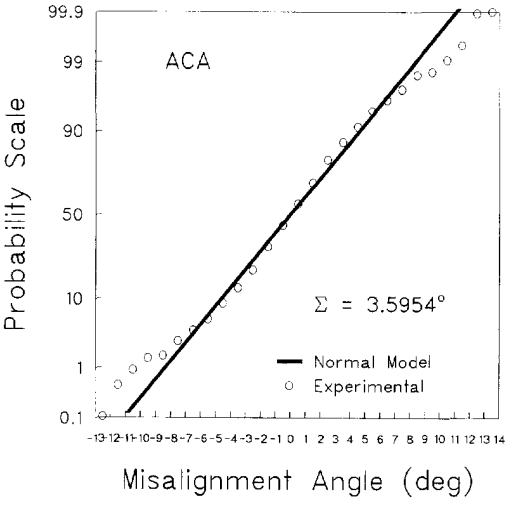

Fig. 4. Probability scale plot of the experimental misalignment data and the normal distribution model.

being equal to the misalignment angle. The Cumulative Distribution Function (CDF) $F(t)$ gives the probability of obtaining a value smaller than or equal to some value t. In terms of the normal distribution, the CDF is given by

$$F(t) = \int_{-\infty}^{t} f(x)\mathrm{d}x \tag{3}$$

where $f(x)$ is the density of the normal distribution (eqn 2). Figure 3 shows the CDF for a normal distribution in comparison with the measured distribution of fiber misalignment. If the data is normally distributed, the resulting collection of plotted points will match the cumulative normal distribution, a sigmoid-shaped curve. As seen from Fig. 3, the experimental fiber misalignment measurements using the cumulative distribution function match the proposed normal distribution model almost exactly.

Probability plotting is a subjective method in which the determination of whether or not the data contradict the assumed model is based on visual examination, rather than statistical calculation (Hahn and Shapiro, 1967). The technique provides a graphical representation of the data as well as an evaluation of the reasonableness of the assumed

Table 3. Standard deviation, expected value, and number of measurements

Material reference code	Normal distribution fiber misalignment standard deviation (degrees)	Half normal distribution expected value (degrees)	Number of measurements
CAA	3.4567	2.758	1271
CAB	3.3875	2.7028	1349
CAC	3.3012	2.634	1280
CBA	3.5308	2.8172	1312
CBB	3.3	2.6331	1224
CBC	3.2795	2.6167	1201
CCA	3.3957	2.7094	1300
CCB	3.0542	2.4369	1170
CCC	3.1796	2.537	1282
ACA	3.5954	2.8688	1359
BCA	3.3651	2.685	1224
CBB	3.3	2.6331	1224

probability model. Basically, if the assumed model is correct, the plotted points will fall in a straight line. If the model is inadequate, the plot will not be linear and the extent and type of departures will be seen.

As seen from Fig 4, the normal distribution appears to be a sufficient model for the fiber misalignment due to the linearity of the plot. Note also the variance of the points in the tails (extreme high or low plotted values) was higher than that of the points at the center of the distribution as expected. As pointed out by Hahn and Shapiro (1967), this variance in the tails of the distribution should not be viewed as a basis on which to reject an assumed model. The standard deviation for all materials considered in this investigation is reported in Table 3 along with the number of measurements taken from each specimen. The number of measurements of individual fiber misalignment was determined so that the expected value of the half normal distribution has a 95% confidence interval of $\pm 0.2^{\circ}$. These measurements were obtained using a video acquisition system. Therefore, a limited number of fields of view were used in the measurements. With a magnification of 200C, approximately 30 to 40 measurements were taken from each field of view. The fields of view were selected randomly.

Fiber micro-buckling occurs at the same load for positive or negative misalignment angle. Therefore, for application of the normal distribution to the problem of compression strength, it was necessary to convert the symmetric normal distribution to a half normal which is a special case of the more general folded normal distribution (Leone *et al.*, 1961; Elandt, 1961). In the half normal distribution, the random variable α is given as $\alpha = \text{abs}(x)$, where x is the random variable of the regular normal distribution. In other words, the half normal distribution represents the normal distribution without the algebraic sign (negative side gets folded onto the positive side). Using the new random variable α, the density of the half normal distribution is derived as (Leone *et al.*, 1961):

$$f(\alpha) = \frac{1}{\Sigma}\sqrt{\frac{2}{\pi}}\exp\left(\frac{-\alpha^2}{2\Sigma^2}\right); \quad \alpha \geqslant 0 \tag{4}$$

Equation 4 has two distinct meanings in the context of fiber reinforced composites (Barbero and Kelly, 1993; Kelly and Barbero, 1993). First, eqn (4) represents the probability that a fiber picked at random in the cross section has a misalignment of value α. But more importantly, assuming that the number of fibers in the cross section is large, eqn (4) gives the ratio of the number of fibers that have a misalignment α over the total number of fibers. By having a large number of fibers in the cross section, there is certainty that a number of fibers with misalignment α will be found. From the statistical representation, it is not possible to say which fibers have that particular value of misalignment but it is possible to assert that a number of them, proportional to $f(\alpha)$, are present in the cross section.

From a probabilistic point of view, the response of the composite may be represented by a model in which all the fibers are assumed to be misaligned the same amount. The single value of misalignment that represents the population (fibers) is the expected value $E(\alpha)$ of the half normal distribution. The standard deviation Σ of the normal distribution should not be used as a representative value of the population because Σ represents a measure of the dispersion, not a representative value of the population. The expected value of a half normal distribution is

$$E(\alpha) = \int_0^\infty \frac{1}{\Sigma}\sqrt{\frac{2}{\pi}}\exp\left(\frac{-\alpha^2}{2\Sigma^2}\right)\alpha\,d\alpha = \sqrt{\frac{2}{\pi}}\Sigma \tag{5}$$

The expected value $E(\alpha)$ for the materials tested in this study range from 2.4° to 2.9° depending on the particular material (Table 3). However, using the expected value did not lead to a good correlation with experimental data.

IMPERFECTION SENSITIVITY EQUATION

Buckling of perfectly aligned fibers was assumed by Rosen (1965). Since experimental data gives lower values of compression strength, many authors have assumed that the buckling load of the fibers is lower than that of the perfect system (Rosen's model) because of fiber misalignment. From stability theory, such behaviour is typical of an imperfection sensitive system. Using stability theory, the authors (Tomblin, 1994) have demonstrated that fiber micro-buckling is imperfection sensitive if the shear stress-strain behavior of the composite is non-linear.

The relationship between the buckling stress (compression strength) and the imperfection magnitude (misalignment) is known in stability theory as the imperfection sensitivity curve. Several models from the literature were used by the authors to develop this type of curve (Tomblin, 1994) but none of the existing models uses the hyperbolic tangent equation (eqn 1) to represent the non-linear shear response. The authors have shown (Tomblin, 1994) that the predictions are very sensitive to the shear equation used to represent the data. Even truncating eqn (1) with a third-order polynomial leads to significant discrepancies with the shear stress-strain data (Fig. 1) for values of shear strain that are expected before compression failure. The discrepancy induced by inadequate representation of the shear response becomes evident in the prediction of compression strength. Since eqn (1) was found to be the best representation of the shear data for the materials under investigation, the development of a new model based on stability theory is justified. Also, existing equations could not be used in the stability analysis because they produced an unsymmetric bifurcation point. Unsymmetric bifurcation means that, because of the shear equation used, a straight fiber would have a preference for buckling with lateral deflections to one side and not to the other, which is physically unrealistic.

A new model, based on the representative volume element of Fig. 5, and similar to the model presented by Wang (1978) is developed here but using the representation of the shear response given by eqn (1). Unlike Wisnom's model (Wisnom, 1990), the model developed in this work incorporates a realistic representation of the sinusoidal fiber pattern, by using a representative volume element (RVE), as shown in Fig. 5, and an energy formulation. Unlike equilibrium-based models that compute the shear strain only at the inflection points (Fig. 5), the shear energy of the entire RVE is represented in the energy formulation used in this section. The assumption of same misalignment for all the fibers is implicitly accepted in all models existing in the literature that use a representative volume element (RVE). The half normal distribution of misalignment will be incorporated later by using damage mechanics concepts.

The model presented in this section is based on the principle of total potential energy and, for simplicity, axial effects are assumed negligible. The in-extensional assumption is widely accepted in stability theory. The shear strain caused by a shear mode of micro-buckling is $\gamma_{xz} = dw/dx$. The constitutive equation is given by eqn (1). The total potential

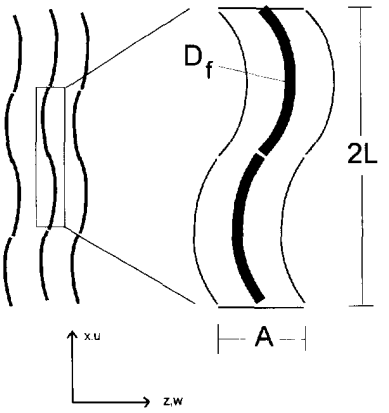

Fig. 5. Representative volume element (RVE).

energy is discretized by writing the lateral deflection as $w = Q_1 \cos(x/l)$ in terms of one degree of freedom Q_1, which represents the amplitude of the lateral deflection. The total potential energy integral is approximated with sufficient accuracy using a four-interval trapezoidal rule. The equilibrium of the system is found by setting to zero the first derivative of the total potential energy with respect to the generalized coordinate Q_1 and solving for the applied stress. In this way, an explicit relationship for the applied stress in terms of the misalignment angle α and the shear strain γ is obtained as,

$$\sigma = \frac{\tau_u}{2(\gamma+\alpha)} \cdot \frac{(\sqrt{2}-1)(e^{\sqrt{2}\gamma G_{LT}/\tau_u} - e^{2\gamma G_{LT}/\tau_u}) + (\sqrt{2}+1)(e^{(2+\sqrt{2})\gamma G_{LT}/\tau_u} - 1)}{1 + e^{2\gamma G_{LT}/\tau_u} + e^{\sqrt{2}\gamma G_{LT}/\tau_u} + e^{(2+\sqrt{2})\gamma G_{LT}/\tau_u}} \tag{6}$$

Typical results are shown in Fig. 6 for two types of shear stress-strain behavior. Note that, if the shear behavior is linear, (constant shear stiffness) the model predicts no critical value (maximum) of stress. On the contrary, by using the hyperbolic tangent representation of shear (eqn 1), a maximum is shown that corresponds to the compression strength for that particular angle of misalignment. The maxima of the curve for all misalignment angles can be found by taking a derivative of eqn (6) with respect to the shear strain, setting it to zero, and solving for the critical shear strain. Putting the critical shear strain back into eqn (6) gives the maxima of the applied stress, which is the compression strength, as a function of misalignment. This process was performed using a symbolic manipulator (Maple V). Because of the complexity of the expressions involved, an implicit solution of the form

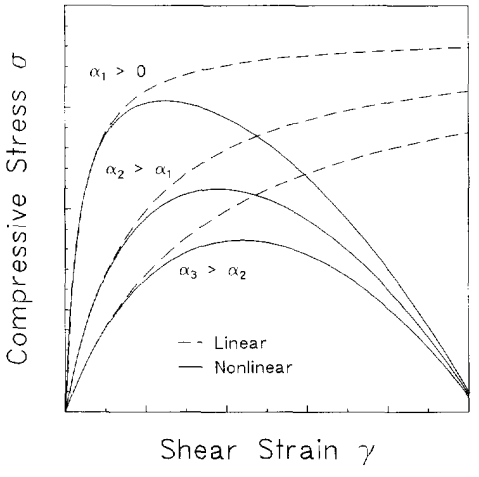

Fig. 6. Equilibrium path showing the applied compression stress as a function of shear strain for three values of the misalignment angle and considering linear shear response (dashed line) and nonlinear shear response (solid line).

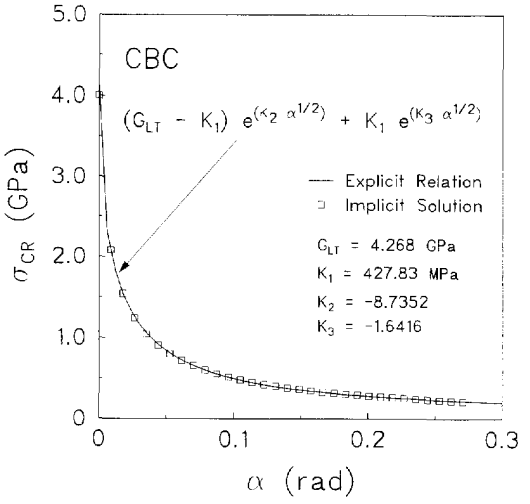

Fig. 7. Imperfection sensitivity plot. Implicit solution $F(\sigma_{CR}, \alpha) = 0$ and explicit solution $\sigma_{CR} = f(\alpha)$.

$F(\sigma_{CR},\alpha) = 0$ was found. Since an explicit solution $\sigma_{CR} = f(\alpha)$ is desired, the implicit solution was fitted with

$$\sigma_{CR}(\alpha) = (G_{LT} - k_1) \exp(k_2\sqrt{\alpha}) + k_1 \exp(k_3\sqrt{\alpha}) \tag{7}$$

where k_1, k_2, and k_3, are constants determined by curve fit of the implicit solution. Equation (7) displays the following characteristics: as $\alpha \to 0$, $\sigma_{CR} \to G_{LT}$, which is Rosen's prediction, and taking into account actual values of k_2 and k_3, as $\alpha \to \pi/2$, $\sigma_{CR} \to 0$. The fit is obtained minimizing the chi-square test statistic with aid of the conjugate gradient technique (Press, 1990) (Quattro Pro). A comparison between the implicit and explicit equations is shown in Fig. 7. The plot in Fig. 7 is known as the imperfection sensitivity curve and eqn (7) is known as the imperfection sensitivity equation.

DAMAGE MODEL

In a previous work (Tomblin, 1994), the authors have demonstrated that a fiber that buckles has no post-buckling strength. The proof does not imply or assume that a buckled fiber is permanently damaged, nor that the process is irreversible. It just indicates that load carrying capacity of a buckled fiber is much lower than the applied load. The fiber may break in a bending mode (Steif, 1990) when the lateral deformation is large. However, the one-dimensional damage model (Kachanov, 1990) presented in this section does not require that the fiber be permanently damaged. It is sufficient to assume that every fiber that has buckled carries no more load because it has no post-buckling strength.

According to the imperfection sensitivity curve in Fig. 7, those fibers that have a large misalignment angle will buckle under relatively low applied stress. Once a fiber buckles, it carries no more load because it does not have post-buckling strength. The applied stress is redistributed onto the remaining fibers that have not buckled. which carry a higher effective stress. At any time during loading of the specimen, the applied load (applied stress times initial fiber area) is equal to the effective stress times the area of fibers that remain unbuckled,

$$\sigma_{\text{app}} = \sigma_{CR}(\alpha)[1 - \omega(\alpha)] \tag{8}$$

where $0 \leqslant \omega(\alpha) \leqslant 1$ is the area of the buckled fibers per unit of initial fiber area. For any value of effective stress, all fibers having more than the corresponding value of misalignment given in Fig. 7 have buckled. The area of buckled fibers $\omega(\alpha)$ is proportional to the area

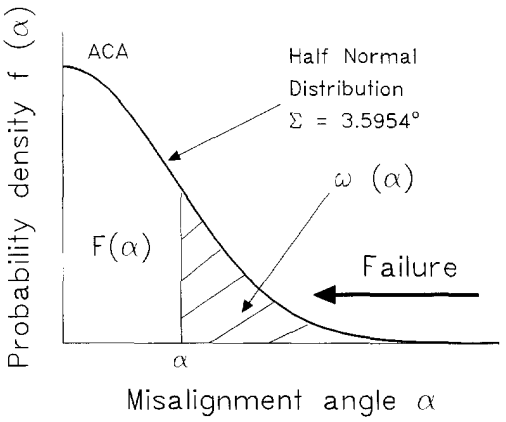

Fig. 8. Half normal probability density distribution of misalignment and interpretation of fiber buckling evolution.

under the half normal distribution (Fig. 8) located beyond the misalignment angle α corresponding to the current effective stress. The total area under the probability density curve (Fig. 8) is equal to one. The area under the curve between $\alpha = 0$ and α is the cumulative probability$F(\alpha)$ corresponding to the probability density of the half normal distribution given in eqn 4. Therefore, $\omega(\alpha)$ is given by

$$\omega(\alpha) = 1 - F(\alpha) = 1 - \int_0^{\alpha} f(\alpha)\,d\alpha = \int_{\alpha}^{\infty} f(\alpha)\,d\alpha \tag{9}$$

Equation (8) has a maximum that corresponds to the maximum stress that can be applied to the composite. The compression strength of the composite is found by setting to zero the derivative of eqn (8) with respect to the fiber misalignment, solving for the critical value of α, and putting it back into eqn (8). These computations were carried out analytically with the aid of a symbolic manipulator (Maple V). The maximum of eqn (8) is a unique value for the compression strength of the composite that incorporates both the imperfection sensitivity curve (Fig. 7) and the distribution of fiber misalignment (Fig. 8).

EXPERIMENTAL COMPRESSION STRENGTH AND CORRELATION WITH THE DAMAGE MODEL

Because of the inherent variability of experimental compression strength data, eight replicates per material were used. Furthermore, eleven different materials had to be tested, which makes the total number of samples to be tested quite large. Therefore, a simple test method was desired. The simple cylindrical geometry of the samples facilitated machining of flat ends that were perpendicular to the axis of the sample. Therefore, experimental compression strength data of rod samples was obtained using a modified ASTM D-695 test fixture (Sonti, 1992). The new fixture is an end-loading fixture like the ASTM D-695 but it uses a special end-constraint grip that prevents bearing failure (end brooming) while avoiding the stress concentration typical of shear loaded fixtures.

Using short samples (38 mm) avoided the need for lateral support. The estimated length for specimen buckling under a fixed end-condition is eight times the length used in the test. The gage section spans the entire length of the specimen. Alignment of the specimens was checked with back-to-back strain gages on half of the samples. A further modification of the D-695 is the alignment system that helps align each sample automatically.

Compression failures were obtained at the center of the gage section, in approximately 75% of the samples. The samples that failed near the ends had compression strength values within the scatter of the remaining tests. The compression strength data compares well with data for glass composites available in the literature (Lo and Chim, 1992). The mean value

Table 4. Comparison of theoretical and experimental compressive strength

Material reference code	σ_{theory} (MPa)	$\sigma_{exper.}$ (MPa)
CAA	369.29	477.74(±36.6)
CAB	341.49	462.65(±16.6)
CAC	364.91	489.74(±26.4)
CBA	410.89	481.04(±25.7)
CBB	432.65	521.56(±16.2)
CBC	433.97	540.34(±20.0)
CCA	393.51	523.74(±16.1)
CCB	422.81	546.28(±10.7)
CCC	388.79	494.88(±15.3)
ACA	434.16	560.90(±35.1)
BCA	439.60	537.05(±39.3)
CBB	490.76*	521.56(±16.2)

* Rectangular sample.

and the 95% confidence interval for each of the eleven materials are shown in Table 4. Eight specimens were tested for each material combination. Also known in Table 4 are the theoretical values computed with the damage model. When G_{LT} and τ_u are measured from torsion data, the predicted compression strength values are 14–25% lower than the experimental strength. The values of τ_u measured with the Iosipescu shear test (Iosipescu, 1967) are higher (Table 2), leading to a predicted strength only 6% lower than the experimental strength (last row of Table 4). The experimental determination of the shear properties needs further investigation.

It must be emphasized that the predicted results are based on measured values for all the parameters that enter into the damage model. The parameters are: the initial shear stiffness G_{LT}, the shear strength τ_u, and the standard deviation of fiber misalignment Σ. All these parameters were measured near the same location on a pultruded rod that showed very consistent properties along its length.

The following conclusion can be drawn from the experimental data. A clear correlation can be seen in Fig. 9 between initial shear stiffness and compression strength, as it was the case in the work of Crasto. However, it is still possible that inter-laminar shear strength may also correlate with initial shear stiffness and compression strength. Further study needs to be done in this direction.

Compression strength as a function of the standard deviation Σ of fiber misalignment is shown in Fig. 10. Clearly, the compression strength decreases with increasing fiber misalignment as shown in Fig. 10. The multi-tow roving with 56 yield obviously induces larger misalignment because of its inherent micro-catenary. The decrease in compression

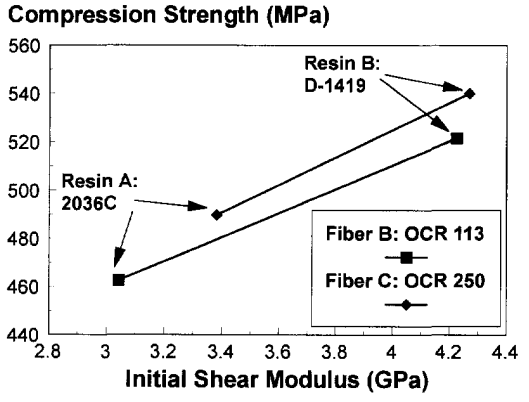

Fig. 9. Influence of initial shear stiffness G_{LT} on compression strength.

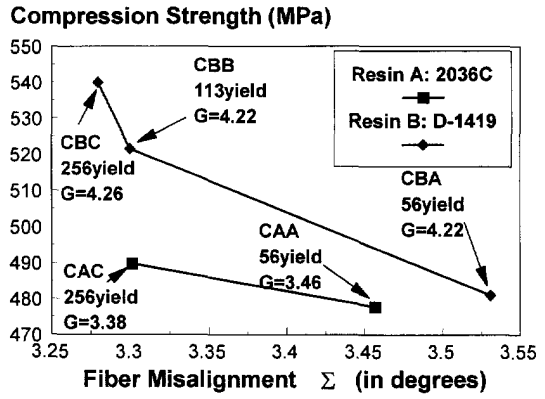

Fig. 10. Influence of fiber misalignment on compression strength.

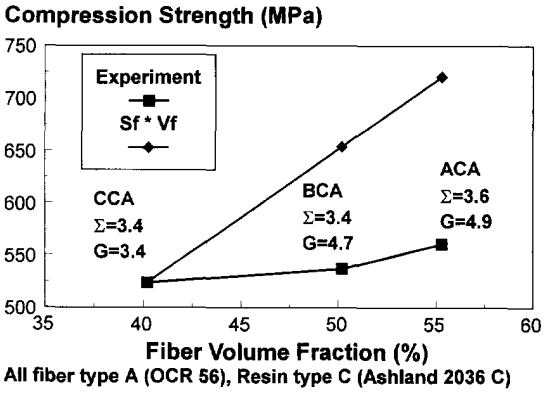

Fig. 11. Influence of fiber volume fraction V_f on compression strength.

strength for the polyester matrix composite with 56 yield fiber is partially compensated by an increase in the initial shear stiffness, as it can be seen in Fig. 10 and Tables 1–4.

Compression strength as function of fiber volume fraction is shown in Fig. 11 for a polyester matrix composite with 56 yield fibers. The plot $S_f \cdot V_f$ represents a linear function of the fiber volume fraction with reference to the strength of the composite with 40.2% fiber volume fraction. The linear plot is included to show that compression strength does not increase linearly with fiber volume fraction. Note that, while the initial shear stiffness of all the composites shown in Fig. 11 are very similar, the fiber misalignment values are quite different. The expected increment in compression strength for higher fiber volume fraction is not realized because of the higher misalignment observed in the materials with higher fiber volume fraction.

CONCLUSIONS

A compression strength model without any semi-empirical parameters has been presented. The model uses only three material parameters that can be measured by well established methodology. The compression strength and all the parameters that enter into the model were measured for the same material. Correlation between predicted values and experimental data for eleven different E-glass reinforced pultruded composites was very good. The effect on inter-laminar shear strength could not be evaluated in this investigation because resins commonly used in pultrusion have similar values of inter-laminar shear strength. Further work needs to be done in this area. Also, the relationship between misalignment in the composites and its causes, including fiber micro-catenary, was not quantified. Further work in this direction is needed because there is significant potential for increasing compression strength by reducing fiber misalignment. Since the compression

strength is sensitive to both shear stiffness and strength, further work is needed on the analytical prediction and experimental determination of shear properties.

REFERENCES

Barbero, E. J. and Kelly, K. W. (1993). Predicting high temperature ultimate strength of continuous fiber metal matrix composites. *J. Composite Mat.* **27,** 1214–1235.

Beltzer, J. G. and Matthews, F. L. (1994). A micromechanics model for compressive failure of unidirectional fiber-reinforced plastics. *J. Composite Mat.* **28,** 1618–1639.

Budiansky, B. (1983). Micromechanics. *Comput. Structures* **16,** 3–12.

Budiansky, B. and Fleck, N. A. (1993). Compressive failure of fiber composites. *J. Mech. Phys. Solids* **41,** 183–211.

Camponeschi, E. T. (1990). Compression response of thick-section composite materials. *SME*-90/90, David Taylor Research Center Report, Bethesda, MD.

Crasto, A. S. and Kim, R. Y. (1990). Compression strengths of advanced composites from a novel mini-sandwich beam. In *22nd Int. SAMPE Technical Conf.* 6–8 November.

Crasto, A. S. and Kim, R. Y. (1992a). Longitudinal compression strength of glass fiber-reinforced composites. In *47th Annual Conf.*, Composites Institute, The Society of the Plastics Industry 3–6 February.

Crasto, A. S. and Kim R. Y. (1992b). The effects of constituent properties on the compression strength of advanced composites. *ASTM Symp. Compression Response of Composite Structures*, 16–17 November.

Chung, I. and Weitsman, Y. (1994). A mechanics model for the compressive response of fiber reinforced composites. *J. Solid Structures* **31,** 2519–2536.

Chung, I. and Weitsman, Y. (1995). On the buckling/kinking compressive failure of fibrous composites. *Int. J. Solid Structures* **32,** 2329–2344.

Elandt, R. C. (1961). The folded normal distribution: two methods of estimating parameters from moments. *Technometrics* **3,** 551–562.

Haberle, J. G. and Matthews, F. L. (1994). A micromechanics model for compressive failure of unidirectional fibre-reinforced plastics. *J. Composite Mat.* **28,** 1618–1639.

Hahn, G. S. and Shapiro, S. S. (1967). *Statistical Models in Engineering*, John Wiley and Sons, NY.

Hahn, H. T. and Williams, J. G. (1986). Compression failure mechanisms in unidirectional composites. In *Composite Materials: Testing and Design (Seventh Conference)*, *ASTM STP* 893, Philadelphia, PA: American Society for Testing and Materials, pp. 115–139.

Iosipescu, N. (1967). New accurate procedure for shear testing of metals. *J. Mat.* **2,** 537–566.

Kachanov, L. M. (1990). *Introduction to Continuum Damage Mechanics*, Kluwer Academic Publishers, Hingham, MA.

Kelly, K. and Barbero, E. J. (1993). The effect of fiber damage on the longitudinal creep of CFMMC. *Int. J. Solids Structures* **30,** 3417–3429.

Kiriakides, R., Arseculeratne, E. J., Perry, E. J. and Leichti, K. (1995). On the compression failure of fiber reinforced composites. *Int. J. Solid Structures* **32,** 689–738.

Lagoudas, D. C., Tadjbakhsh, I. and Fares, N. (1991). A new approach to microbuckling of fibrous composites. *J. Applied Mech.* **58,** 473–479.

Lagoudas, D. C. and Saleh, A. M. (1993). Compressive failure due to kinking of fibrous composites. *J. Composite Mat.* **27,** 83–106.

Leone, F. C., Nelson, L. S. and Nottingham, R. B. (1961). The folded normal distribution. *Technometrics* **3,** 543–550.

Luciano, R. and Barbero, E. J. (1994). Formulas for the stiffness of composites with periodic microstructure *Int. J. Solids Structures* **31,** 2933–2944.

Lo, K. H. and Chim, E. S.-M. (1992). Compressive strength of unidirectional composites. *J. Reinforced Plastics Composites* **11,** 838–895.

Madukar, M. S. and Drzal, L. T. (1992). Fiber-matrix adhesion and its effect on composite mechanical properties: longitudinal compression properties of Graphite-Epoxy. *J. Composite Mat.* **26,** 311–333.

Maewal, A. (1981). Post-buckling behavior of a periodically laminated medium in compression. *Int. J. Solids Structures* **17,** 335–344.

MAPLE V (1991). Waterloo Maple Software, Waterloo, ON Canada.

Mrse, A. and Piggott, M. R. (1990). Relation between fibre divagation and compressive properties of fibre composites. *35th Int. SAMPE Symp.* 2–5 April, pp. 2236–2244.

Piggott, M. R. (1981). A theoretical framework for the compressive properties of aligned fibre composites. *J. Mat. Science* **16,** 2837–2845.

Press, W. H., Flannery, B. P., Teukolsky, S. A. and Vetterling, W. T. (1990). *Numerical Recipes*, Cambridge University Press, New York, NY.

QUATTRO-PRO (1993). Borland International, Inc., Scotts Valley, CA.

Rosen, B. W. (1965). *Fiber Composite Materials*, American Society for Metals, Metals Park, OH.

Shuart, M. J. (1985). Short-wavelength buckling and shear failures for compression loaded composite laminates. *NASA TN*-87640, NASA Langley Research Center, Hampton, VA, U.S.A.

Steif, P. S. (1987). An exact two-dimensional approach to fiber microbuckling. *Int. J. Solids Structures* **23,** 1235–1246.

Steif, P. S. (1990). A model for kinking in fiber composites—part I: fiber breakage via micro-buckling; part II: kink band formation. *Int. J. Solids Structures* **26,** 549–561, 563–569.

Sonti, S. (1992). Stress analysis of pultruded structural shapes. Thesis, West Virginia University, Morgantown, WV, U.S.A.

Sonti, S., Barbero, E. J. (1995). Material characterization of pultruded laminates and shapes. *J. Reinf. Plast. Comp.*, in press.

Sun, C. T. and Jun, A. W. (1993). Effect of matrix nonlinear behavior on the compressive strength of fiber composites. In *Mechanics of Thick Composites, the 1st Joint meeting of the ASME-ASCE-SES: Meet'N'93*. Charlottesville, VA. 6–9 June, pp. 91–105.

Tang, J. M., Lee, W. I. and Springer, G. S. (1987). Effects of cure pressure on resin flow, voids and mechanical properties. *J. Composite Mat.* **21,** 421–440.

Tomblin, J. S. (1994). Compressive strength models for pultruded glass fiber reinforced composites. Ph.D. dissertation, West Virginia University, Morgantown, WV, U.S.A.

Wang, A. S. D. (1978). A non-linear microbuckling model predicting the compressive strength of unidirectional composites. *ASME Paper* 78-*WA/Aero*-1, ASME Winter Annual Meeting.

Wisnom, M. R. (1990). The effect of fibre misalignment on the compressive strength of unidirectional carbon fiber/epoxy. *Composites* **24,** 403–407.

Yeh, J. R. and Teply, J. L. (1988). Compressive response of Kevlar/epoxy composites. *J. Composite Mat.* **22,** 245–257.

Yurgartis, S. W. (1987). Measurement of small angle fiber misalignments in continuous fiber composites. *Composites Sci. Tech.* **30,** 279–293.

Yurgartis, S. W. and Sternstein, S. S. (1992). Experiments to reveal the role of matrix properties and composite mircostructure in longitudinal compression strength. *ASTM Symp. Compression Response of Composite Structures*. 16–17 November.